www.amlett.com, www.vbripress.com/aml, DOI: 10.5185/amlett.2015.5776 Published online by the VBRI Press in 2015

Visible light driven photocatalytic degradation of the reactive red-198, methylene blue and 3-chloro phenol by Nb_2O_5@Zno: Synthesis and characterization

K. Chennakesavulu[1*], G. Ramanjaneya Reddy[2], S. Sanjeevi Prasath[3], S. Supriya[1], S. Sivanesan[3]

[1]*Department of Chemistry & Centre of Excellence in Energy Research, International Research Centre, Sathyabama University, Jeppiaar Nagar, Chennai 600 119, India*
[2]*Department of Inorganic Chemistry, School of Chemical Sciences, University of Madras, Guindy Campus, Chennai 600 025, India*
[3]*Centre for Nanoscience and Nanotechnology, International Research Centre, Sathyabama University, Chennai 600 119, India*

[*]Corresponding author. Tel: (+91) 4424503814; E-mail: chennanml@yahoo.com

Received: 13 December 2014, Revised: 15 March 2015 and Accepted: 18 March 2015

ABSTRACT

In-situ synthesis of ZnO and Nb_2O_5 composites was carried out in alkaline medium. The obtained composites were characterized by Fourier transform infrared spectroscopy (FTIR), Raman spectroscopy, diffuse reflectance UV-Vis spectrophotometer (DRS), Powder X-ray diffraction (XRD), X-ray photoelectron spectroscopy (XPS), Brunauer-Emmett-Teller (BET) surface area method, N_2-sorption isotherms, Thermo gravimetric analysis (TGA), Particle size and Field emission scanning electron microscopy (FESEM/EDX). The synthesized composite was used as photocatalyst in the degradation of reactive red-198 (RR), methylene blue (MB) and 3-chloro phenol (3CP) under visible light irradiation. The catalytic activity and removal percentage of dye was determined by the spectrophotometric method, it indicates high percentage of degradation for the ZnO:Nb_2O_5 composite. The kinetic parameters were found to obey *pseudo*-first order oxidation reaction, which may be due to the fixed amount of the catalyst and concentration of the dye solution. The recycled and purified composites of ZnO:Nb_2O_5 was tested the catalytic activity and was compared with that of the fresh catalyst. Copyright © 2015 VBRI press.

Keywords: Zinc oxide; niobium oxide; photocatalyst; visible light; reactive red198; methylene blue; chlorophenol.

Kattela Chennakesavulu graduated from Sri Krishna Devaraya University, Anantapur, Andhrapradesh, India. He received his PhD degree in 2011 from the University of Madras, Chennai, India under the supervision of Dr. Guntamadugu Bhaskar Raju, Chief Scientist, CSIR-NML Madras Centre, CSIR Madras Complex, Chennai, India. Presently he is working as Assistant Professor in Department of Chemistry & Centre of Excellence in Energy Research, International Research Centre, Sathyabama University. His research interest includes chemistry of calixarenes, mineral processing, nanomaterials, catalysis, and mesoporous materials.

Sridhar Sanjeevi Prasath graduated from Thiruvalluvar University, Vellore, Tamilnadu, India. He completed post graduation in Chemistry from the University of Madras, Chennai, India. Presently he is working as Junior Research Fellow at Centre for Nanoscience and Nanotechnology in Sathyabama University, Chennai, India. His research interest includes synthesis of nanomaterials and photonic crystals.

Gontu Ramanjaneya Reddy graduated from the Acharya Nagarjuna University, Guntur, Andhrapradesh, India. He received Post graduation in Chemistry from Bharathidasan University, Trichy, Tamilnadu, India. Currently he is pursuing PhD at University of Madras, Chennai, India. His research is primarily focused on inorganic metal complexes, bio-inorganic chemistry, catalysis and nanomaterials.

Introduction

Niobium and niobium oxide containing composites were one of the most significant semiconducting refractory materials **[1, 2]**. The Nb, Ta and their oxides do not occur naturally as free metals and most of these oxides are minerals and silicates for example Columbite, Leushite, and Loparite [**3, 4**]. Nb and Ta have high durability, electrical resistivity, corrosive resistance, super conductivity, surface area and melting point etc. The usage of Nb and Ta was essential in catalysis, sensors, optics, coatings, batteries,

drug delivery, gene delivery, photonics and microelectronics. The Nb and Ta based composites show higher catalytic activity than ZnO, Fe_3O_4, CuO, CeO_2, and TiO_2 **[5-8]**. The composite materials were used as eco-friendly heterogeneous catalyst in many organic transformations **[9-10]**. The Co doped ZnO nanodisks were synthesized by chemical method and the photocatalytic activity was checked against methyl orange under visible irradiation. The results show that the complete degradation of methyl orange take place within 8 minutes. Recently the Fe, Cu doped ZnO nanoparticle used as a photocatalyst in the degradation of methylene blue in presence of 30% H_2O_2 under visible light and the results shows that the composite has three times more efficient than ZnO. The V and Nb doped ZnO were systematically investigated by using hybrid functional calculations. The Nb doped ZnO m has significant visible light absorption. The soil derived microorganism Rhizopus oryzae was used to remove the reactive red -198 and 96% was achieved under optimal conditions **[11-14]**. The degradation of cationic dyes such as rhodamine-B, rhodamine-6G, methylene blue, reactive red-198, chloro-phenols, by ZnO is very slow under visible light irradiation. The catalytic activity of ZnO could be increased by doping with oxides of Nb and Ta. The Nb in the d^0 configuration, it possesses + 5 oxidation states, so there is a valence difference exist between Zn^{+2} and Nb^{+5}, this allows the Nb atoms to contribute multiple electrons. The Nb_2O_5-ZnO hierarchical structure can perform well when used as catalysts in the degradation of model toxic dyes **[15, 16]**.

In the present investigation, in-situ chemical synthesis of Nb_2O_5:ZnO composites with different wt% of Nb in basic medium are made. The synthesized composite materials were well characterized and used as photo catalyst in the degradation of reactive red-198, methylene blue and 3-chloro phenol under visible light irradiation. Spectrophotometeric method was used for the determination of percentage degradation during the degradation. The recovered catalysts catalytic activity also compared that of fresh catalyst.

Experimental

Materials

Zinc chloride (99.8%), ammonia (35%), 3-chlorophenol (99%) Merck Pvt. Ltd, India, methylene blue (<100%), niobium penta chloride (99%), (Sigma-Aldrich Pvt. Ltd, India) and reactive red-198 (Textile industry, Tamilnadu) were used and other analar grade chemicals were used without further purification. Millipore water was used throughout the work.

Methods

The FTIR spectra were recorded on a FTIR Perkin-Elmer 8300 spectrometer with KBr disk. The UV-Vis absorption spectra of liquid samples were recorded on a Perkin Elmer Lambda-35 spectrophotometer. The UV-Visible Diffuse Reflectance Spectral (UV-Vis/DRS) analyses were carried out on a JASCO-V-670 UV-visible spectrophotometer. Raman spectra were recorded on a NANO PHOTON11i confocal Raman microscope using a He-Ne laser emitting at 532 nm. The crystalline nature of the ZnO-Niobium composites was ascertained by powder X-ray diffraction using Rigaku XRD-Smart Lab with Cu-$K\alpha_1$ radiation (λ=1.5418 Aº). TGA experiments were performed with Versa Therm Cahn Thermo balance TG-151 with a sensitivity of 10μg. TGA experiments were conducted in the temperature range of 30-900 °C with 20 ± 0.01 mg of the samples and the analyses were carried out at a heating rate of 10 °C/ min under static air atmosphere. The N_2 adsorption, desorption isotherms and Brunauer-Emmett-Teller (BET) surface area measurements at –196 °C were carried out on a Micrometrics ASAP (Model 2020) surface area analyzer with nitrogen and helium gases with a purity of 99.99% **[17]**. The FESEM was obtained on a FESEM-SUPRA 55-CARL ZEISS scanning electron microscope. The XPS analysis was carried out on Kratos AXIS 165 XPS system with Mg-Kα monochromatic wavelength. All the samples were made into pellets and were used as such for X-ray Photoelectron Spectroscopic (XPS) studies. The high resolution XPS traces were deconvoluted using the Gaussian statistical analysis by using origin-7 software. The particle size distribution of the composites was analyzed with dispersion technology, zeta acoustic sizer (DT 1200).

Synthesis of the ZnNb composites

In a double necked round bottom flask 0.05M (6.53gm) of anhydrous zinc chloride was well dispersed in 200 ml of ethanol solution. To this drop wise addition of 0.3 M ammonia solution at room temperature resulted in a white precipitate. The precipitate was centrifuged and washed with milli-Q water, then heated in furnace at 200 ^oC for 4 h. The well dispersed ethanolic solution containing 35 mg/115 mg/175 mg and 245 mg of $NbCl_5$ were added during the synthesis of composites. The resulted sol-gel mixture was centrifuged and washed with milli-Q water. The ZnO and its composites synthesized with 1%, 3%, 5% and 7% of niobium oxide in ZnO are here after represented as $ZnNb_0$, $ZnNb_1$, $ZnNb_3$, $ZnNb_5$ and $ZnNb_7$ respectively.

Photocatalytic degradation of the RR and MB under visible light irradiation

The photocatalytic activities of the $ZnNb_0$, $ZnNb_1$, $ZnNb_3$, $ZnNb_5$ and $ZnNb_7$ in degradation of the RR and MB under visible light in a cylindrical glass reactor with the each catalyst 0.1 g of $ZnNb_0$, $ZnNb_1$, $ZnNb_3$, $ZnNb_5$ and $ZnNb_7$ and 0.01 mmol of 100 mL aqueous dye solution was added to the catalysts separately. The reaction conditions are optimized in dark at room temperature and start irradiation under visible light (> 360 nm). The removal percentage and consequent spectral changes at predetermined time intervals were monitored by the UV-Visible absorption spectra at 521± 1, 664± 1 nm for RR and MB for 3 h and 2.5 h respectively. The percentage conversion is calculated from equation (1).

$$A = \varepsilon c l \quad (1)$$

Here, ε = molar extinction coefficient [M^{-1} cm^{-1}], c = sample concentration, l = path length of cuvette (1 cm).

Photocatalytic degradation of the 3CP under visible light irradiation

The photo catalytic activities of the $ZnNb_0$, $ZnNb_1$, $ZnNb_3$, $ZnNb_5$ and $ZnNb_7$ in degradation of 3CP under visible light in a cylindrical glass reactor with 0.1 g of $ZnNb_0$, $ZnNb_1$, $ZnNb_3$, $ZnNb_5$ and $ZnNb_7$ and 0.001 mmol of 100 mL aqueous dye solution. The reaction conditions are optimized in dark at room temperature and started irradiation of visible light (> 360 nm). The removal percentage and consequent spectral changes at predetermined time intervals were monitored by UV-Visible absorption spectra at 276 ± 1 nm for 3CP for 2 h respectively. The percentage conversion is calculated from equation (1).

Results and discussion

Fourier transform infrared spectroscopy (FTIR)

The FTIR spectra of $ZnNb_0$, $ZnNb_1$, $ZnNb_3$, $ZnNb_5$ and $ZnNb_7$ are given in **Fig. 1(a-e).** The composites show peak in the region of 1658 cm^{-1} due to the in-plane bending vibration of O-H. The bands in the range of 3300-3500 cm^{-1} are due to the surface present hydroxyl groups**.** A strong band at 448 cm^{-1} was assigned to the stretching frequency of Zn-O group [**19**]. In **Fig.1 (b-e),** strong absorption peaks at 3500 cm^{-1} and 1660 cm^{-1} were attributed to the O-H stretching of Nb=O-H_2O(OH) and in-plane bending vibration of Nb-OH [**20].** The characteristic absorption bands in the range of 500-1000 cm^{-1} were assigned to Nb-O stretching and Nb-O-Nb angular vibrations [**21**]. The peak between 510-545 cm^{-1} indicates the stretching vibration of Nb_2O_5 and at this region peak intensity was progressively increased with the increase in the wt% of niobium oxide. The peak after 885 cm^{-1} is assigned for NbO_2 modes and in the region of 900 cm^{-1} the broad band observed, is due to the niobium pentaoxide moieties **[22].** Hence the FTIR studies confirm the presence of niobium oxides along with the zinc oxide nanostructure.

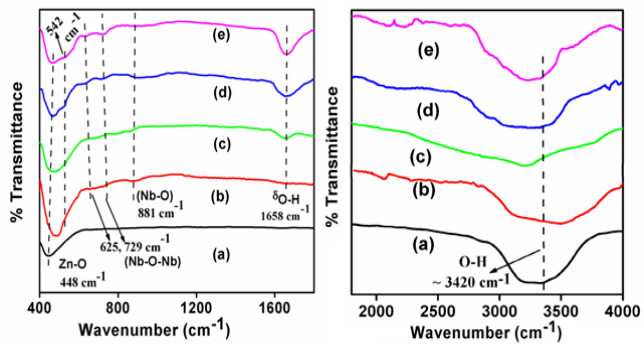

Fig. 1. FTIR spectra of the (a) $ZnNb_0$, (b) $ZnNb_1$, (c) $ZnNb_3$, (d) $ZnNb_5$ and (e) $ZnNb_7$.

DRS UV-visible analysis

The DRS/UV-visible spectra of $ZnNb_0$, $ZnNb_1$, $ZnNb_3$, $ZnNb_5$ and $ZnNb_7$ were recorded in the range of 200-800 nm and the spectral traces are provided in **Fig. S1 (a-e).** It was found that the absorption spectra of ZnO loaded with niobium salt with different molar ratios spectra were almost same. The absorption edges of all the samples were observed around 358 nm [**23**]. There is no d-d transition within the range of 400-800 nm in the DR/UV-Vis spectra **(Fig. S1),** clearly suggest that niobium is most probably in d^0 configuration corresponding to Nb(V) [**24].** The presence of a band in the region of 220-300 nm was due to the energy transfer of oxygen to metal charge transfer transitions. It indicates the coordination of dimeric niobium oxide in ZnO nanorods.

Raman spectral analysis

Fig. 2 shows the Raman spectrum of all composites in the range of 100-900 cm^{-1}. Three main bands were observed for ZnO nanorods at 390, 421 and 484 cm^{-1}. The band around 382 cm^{-1} may be ascribed to multi-phonon scattering process in ZnO. The band at 415 cm^{-1} shows the characteristic bending mode of wurtzite phase [**25-27].** The asymmetric broad band is the characteristic feature of wurtzite in nanorods form. The band at 567 cm^{-1} corresponds to the A_1 mode of ZnO [**28].** Therefore, the recorded Raman spectrum clearly demonstrates that the ZnO nanorods have a hexagonal wurtzite structure of good crystal quality**.**

The Raman spectra of the $ZnNb_0$, $ZnNb_1$, $ZnNb_3$, $ZnNb_5$ and $ZnNb_7$ catalysts were shown in **Fig. 2.** Raman spectrum of composite shows two weak bands at 150 to 380 cm^{-1} and 720 to 900 cm^{-1}, whereas these bands are absent in the of ZnO. The Raman shift at 760 and 865 cm^{-1} peak intensity increases with doping of Nb_2O_5, it was due to octahedral NbO_6 units [**29].** The region around 885 cm^{-1} corresponds to the stretching modes of Nb-O bond. Raman peak around 285-380 cm^{-1} were assigned to Nb-O-Nb bending vibrations in NbO_6 octahedra and due the oxide of the Nb [**30].** The shift indicates all composites have stable confinement with the ZnO. This is indicates the presence of dimeric form of Nb_2O_5 in ZnO nanorods.

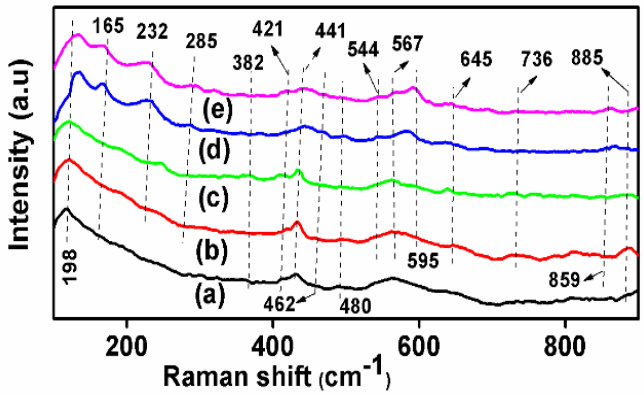

Fig. 2. Raman spectra of the (a), $ZnNb_0$, (b) $ZnNb_1$, (c) $ZnNb_3$, (d) $ZnNb_5$ and (e) $ZnNb_7$.

Powder XRD analysis

The crystalline and crystal phases of the $ZnNb_0$, $ZnNb_1$, $ZnNb_3$, $ZnNb_5$ and $ZnNb_7$ composites were examined by X-ray diffraction and were shown in **Fig. 3 (a-e).** The well defined diffraction reflections appeared in the, this are related to the pure wurtzite hexagonal phase. The characteristic patterns at (1 0 0), (1 0 1), (1 0 2), (1 1 0), (1 0 3), (1 1 2), (2 0 1), (0 0 4) and (2 0 2) were corresponding

to the hexagonal wurtzite phase of ZnO nanorods. These peaks well-matched with the standards [**31, 32].** The XRD patterns of Nb_2O_5 doped ZnO nanorods revealed broadening and lowering of intensity of the peaks. This confirms that the niobium oxide was doped in the wurtzite phase. The crystalline size for $ZnNb_0$ was 24 nm, calculated from the X-ray line broadening using the Scherrer formula.

$$D_p = \frac{0.94 * 1.54056\ A^o}{\beta \cos\theta} \qquad (2)$$

D_p = Average Crystallite size,

β = Line broadening in radians. (0.521 degree),

2θ = Bragg angle (36.3 degree),

λ = X-ray wavelength (1.54056 A^o).

In pure ZnO nanorods, there is no extra peak related to any impurity within the detection limit of the instrument, which confirms that the synthesized ZnO was the pure phase of wurtzite. But in the composites, the new peaks were observed and 2 theta value at 23.5°, 28.3° and very low intense peak at 31.2° indicating the prominent doping of Nb_2O_5. The new peaks at 23.3°, 28.4° with diffraction patterns are (0 0 1), (1 1 0), correspond to the niobium oxide. The shift in peak position was not observed, but a slight change may be due to the different size and crystal nature of both zinc oxide and niobium oxide. At this percentage of doping the crystallinity and the lattice pattern are not affected.

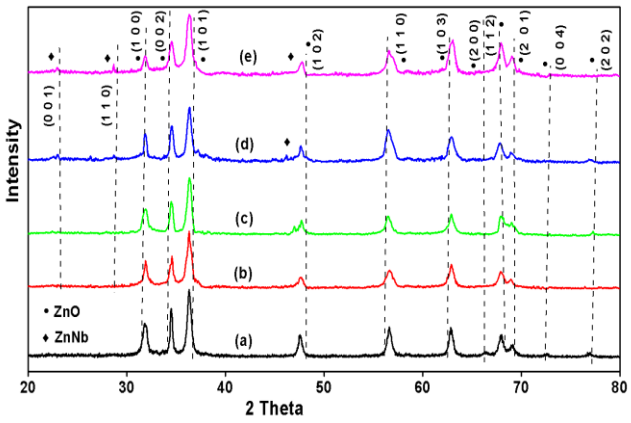

Fig. 3. XRD patterns of the (a) $ZnNb_0$ (b) $ZnNb_1$ (c) $ZnNb_3$ (d) $ZnNb_5$ and (e) $ZnNb_7$.

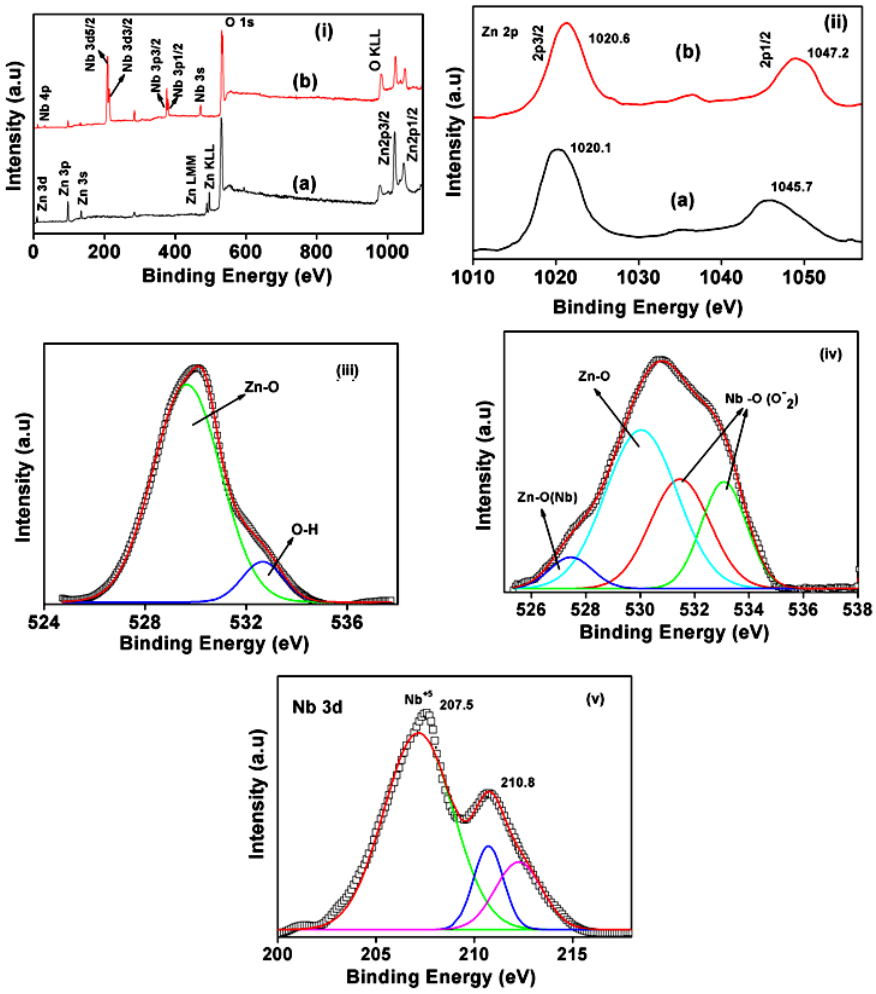

Fig. 4. XPS survey spectra of the (i) (a) survey graphs of the ZnO and (b) $ZnNb_7$ (ii) Zn2p level spectra (iii) & (iv) O1s deconvoluted spectra and (v) Nb 3d spectrum of the ZnO and $ZnNb_7$.

X-ray photoelectron spectroscopy analysis

In order to identify and compare the chemical states of elements in the architecture of ZnNb nanocomposite, the prepared $ZnNb_7$ was subjected for XPS analysis and the results are shown in **Fig. 4**. The XPS studies reveals the presence of Zn(II), Nb(V) and O. The XPS survey scan of the composite shows carbon signal (284.6 eV), which is always present in the spectra. The highly intense broad bands confirm the presence of oxygen. The O 1s, Nb 3d and Zn 2p appear at binding energy values of 531.2, 207.5 and 1022.6 eV respectively [**33]. Fig. 4 (v)** shows the Nb 3d core level spectra and binding energy values at 210.8 eV and 207.5 eV for the Nb $3d_{3/2}$ and Nb $3d_{5/2}$ respectively. This confirms the +5 oxidation state of Nb **Fig. 4 (ii)** shows the peaks at 1020.6 and 1047.2 eV related to Zn $2p_{3/2}$ and Zn $2p_{1/2}$ respectively. The O 1s deconvoluted XPS traces of the ZnO and $ZnNb_7$ are given in **Fig. 4 (iii** & **iv)**. The O 1s core level XPS spectral traces suggests the asymmetric nature and also the deconvoluted spectral trends suggesting that there are more than one oxygen bond with Nb. The O 1s core level spectrum can be fitted with multipeaks, which are characteristic of the oxygen anions (O_2^-) bound to niobium. The lattice (530 eV) and oxygen in hydroxyl groups (532.5 eV)) further confirms the presence of OH groups [**34].** The Nb doped ZnO and ZnO exhibits different oxygen binding properties, which might be due to the formation of dimeric niobium oxide forms with different valence states. The peak at 533.05 is due to the O-Nb=O, the peak 531.4 correspond to the Nb-O groups. The peak around 527.8 eV may be due to the coordination of ZnO with Nb oxides **[35]**. In Zn 2p level spectra, the binding energy difference of 1.46 eV was observed between ZnO and $ZnNb_7$. This confirms the presence of niobium in ZnO nanorods.

Particle size analysis

The particle size distribution curves obtained for the samples $ZnNb_0$, $ZnNb_1$, $ZnNb_3$, $ZnNb_5$ and $ZnNb_7$ in aqueous medium were provided in **Fig. S2**. The particle size distribution curves of the parent pure zinc oxide nanorods shows the mean diameter as 40 nm, where as the $ZnNb_1$, $ZnNb_3$, $ZnNb_5$ and $ZnNb_7$ shows at 46.5, 51.3 54.5, and 62.5 nm respectively. It indicates that, the doping of metal may cause slight aggregation of particle in the aqueous medium.

BET analysis and N_2 sorption isotherms

The Brunauer-Emmett-Teller (BET) surface area N_2 adsorption/desorption isotherms, and the pore volume studies for the $ZnNb_0$, $ZnNb_1$, $ZnNb_3$, $ZnNb_5$ and $ZnNb_7$ are shown in **Fig. 5(a-e)**. The composites have type-IV isotherms, but a steep increase was observed above P/P_o = 0.8. BET surface area of the $ZnNb_0$, $ZnNb_1$, $ZnNb_3$, $ZnNb_5$ and $ZnNb_7$ samples were determined to be 15.7, 12.5, 10.1, 9.2 and 8.1 m^2/gm, respectively. Though the surface area values were reduced, it indicates the formation of ZnNb composites. The pore size distribution curves of samples were evaluated from the adsorption branches of the isotherms given in the inset of **Fig. 5**.

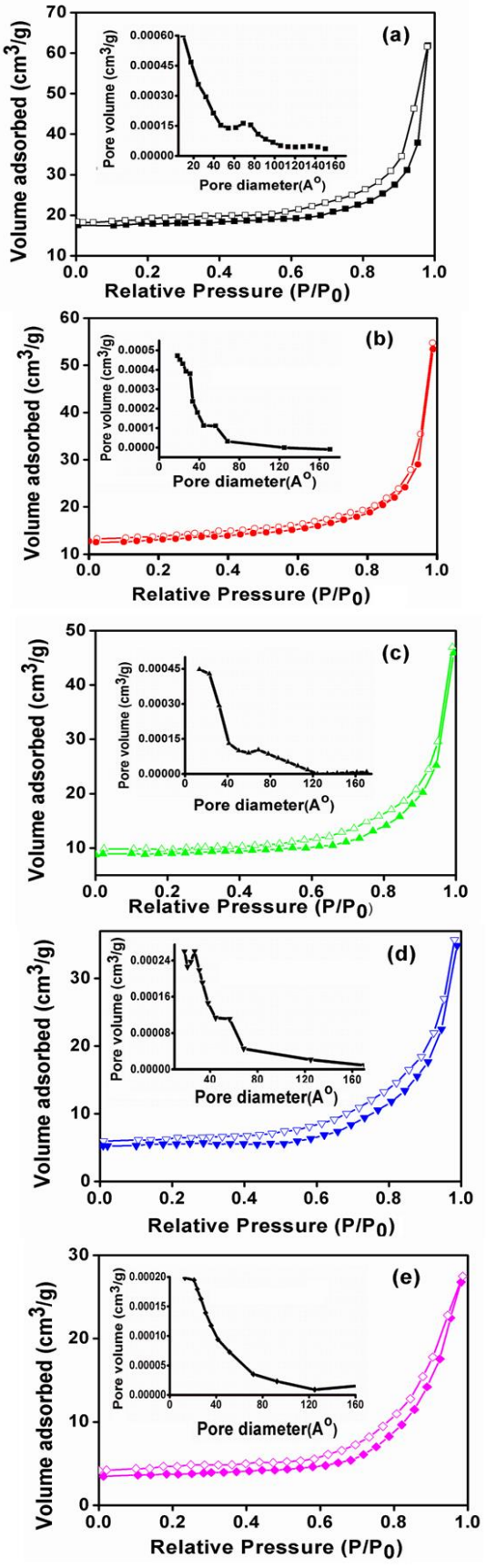

Fig. 5. The N_2 isotherms of the (a) $ZnNb_0$ (b) $ZnNb_1$ (c) $ZnNb_3$ (d) $ZnNb_5$ and (e) $ZnNb_7$, and inset diagrams showing the pore size distribution curves.

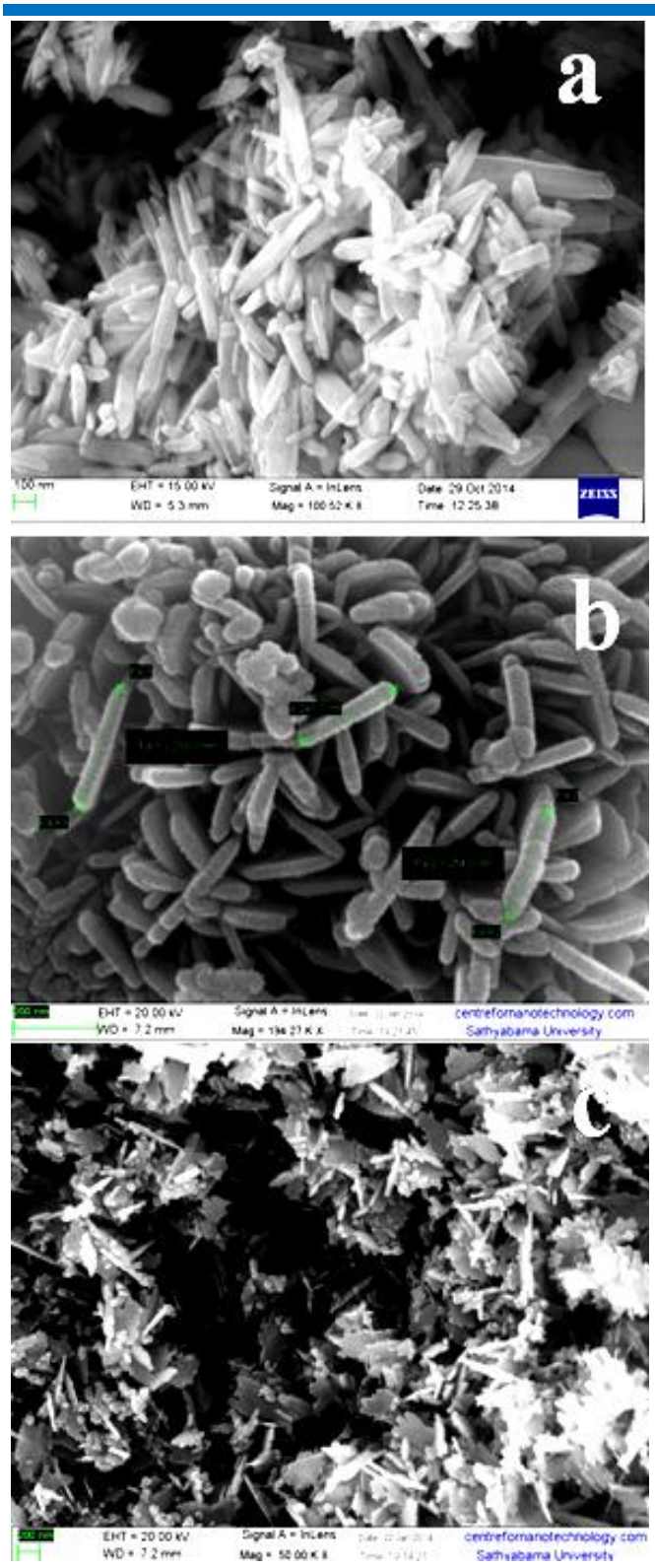

Fig. 6. FESEM patterns of the (a) $ZnNb_0$ (b) $ZnNb_3$ and (c) $ZnNb_7$.

The average pore diameter of ZnO is 40 A^o, but in the case of composite, the average pore diameter values were below 40 A^o. Thus, BET data satisfactorily correlate with the XRD results and the discrepancy between BET and XRD data can be due to the complicated geometry of the polycrystalline nanostructure **[36].**

Electron microscopic analysis

The scanning electron microscopy (SEM) reveals effective doping and purification. **Fig. 6** shows, the morphology analysis of the synthesized ZnNb0, $ZnNb_1$ nanorods and $ZnNb_5$ nanorods. The shape of zinc oxide rod does not change during the doping of niobium oxide. Nb_2O_5 particles are uniformly doped on the surface of the zinc oxide nanorods **[37-39]**. The corresponding EDX **(Fig. S11)** patterns of the ZnNb0, $ZnNb_1$ and $ZnNb_5$ are given in **Fig. 6(a-c)**. The SEM/EDX shows the morphology and effective doping of e niobium on zinc oxide nanorods**.**

Thermal analysis

The TG/DTG curves of $ZnNb_0$, $ZnNb_1$, $ZnNb_3$, $ZnNb_5$ and $ZnNb_7$ in static air atmosphere are shown in **Fig. S3.** Residual mass of the composites are almost same. With increase in the Nb wt%, DTG curves shows multistep decomposition pattern. This clearly suggests the refractory metal niobium enhancing the ZnO thermal stability.

Catalytic studies

Mechanistic issues involved in the degradation of RR, MB and 3CP

The photocatalytic degradation of RR, MB and 3CP with $ZnNb_0$, $ZnNb_1$, $ZnNb_3$, ZnNb5 and $ZnNb_7$ under visible light irradiation has been studied. The percentage of degradation and kinetic parameter were calculated from the equation (1). The rate of reaction follows the first order rate equation.

$$\ln\left(\frac{C_t}{C_0}\right) = -k\ t \qquad (3)$$

Here C_t is the concentration of the dye at different time, C_0 is the initial concentration, t is the time and k is the rate constant in min^{-1}.

The degradation efficiency was calculated by optical absorption spectral analysis. The aliquot samples of the reaction medium were collected and the consequent absorption changes were recorded at 520±1 nm, 664±1 and 275±1 nm for RR, MB and 3CP respectively [**40, 41].** The spectral changes are given in **Fig. S4-S6** (supporting data). The $ZnNb_1$, $ZnNb_3$, $ZnNb_5$ and $ZnNb_7$ have more degradation performance when compared to $ZnNb_0$. From the **Fig. 7(i-iii)** removal percentages of RR are 26%, 63%, 79%, 91% and 100% for the $ZnNb_0$, $ZnNb_1$, $ZnNb_3$, $ZnNb_5$ and $ZnNb_7$ respectively. In case of MB 42%, 71%, 78%, 98% and 100% for the $ZnNb_0$, $ZnNb_1$, $ZnNb_3$, $ZnNb_5$ and $ZnNb_7$ respectively. In the case of 3CP 67% 71% , 82%, 100% and 98 % for the $ZnNb_0$, $ZnNb_1$, $ZnNb_3$, $ZnNb_5$ and $ZnNb_7$ respectively. The ZnNb composites could decrease the recombination of electron-hole pair and enhance the photocatalytic performance. Particle size also has an impact on the activity of the photo catalysts. Here the gradual decrease in the mean particle size may lead to the induced charge transfer in HOMO-LUMO energy levels to prevent electron hole recombination **[42].** The reaction was carried out at fixed concentration of the all reactants. The catalytic reactions exhibit *pseudo*-first order kinetic parameters.

Fig. 7(iv-vi) reveals the negative slope in all cases. The rate constants of RR were 0.0028 min^{-1}, 0.0049 min^{-1}, 0.00739 min^{-1}, 0.013 and 0.020 min^{-1} for $ZnNb_0$, $ZnNb_1$, $ZnNb_3$, $ZnNb_5$ and $ZnNb_7$ respectively. The rate constant of MB were 0.0029, 0.0075, 0.0097, 0.014 min^{-1} and 0.016 for $ZnNb_0$, $ZnNb_1$, $ZnNb_3$, $ZnNb_5$ and $ZnNb_7$ respectively. The rate constant of 3CP were 0.006, 0.007, 0.01, 0.012 min^{-1} and 0.015 for $ZnNb_0$, $ZnNb_1$, $ZnNb_3$, $ZnNb_5$ and $ZnNb_7$ respectively. The photo generated holes and electrons may react with surface hydroxyl groups and adsorbed water or O_2 to generate the active oxidative ionic radicals ($O_2^{\bullet-}$ and $^{\bullet}OH$) from the reaction medium. The $O_2^{\bullet-}$ and $^{\bullet}OH$ radicals are very reactive and quickly oxidise organic species at the surface of the ZnO. Hydroxy radicals ($^{\bullet}OH$) were considered to be the most powerful oxidant (E^o = 2.8 V) amongst other oxidants [**43].**

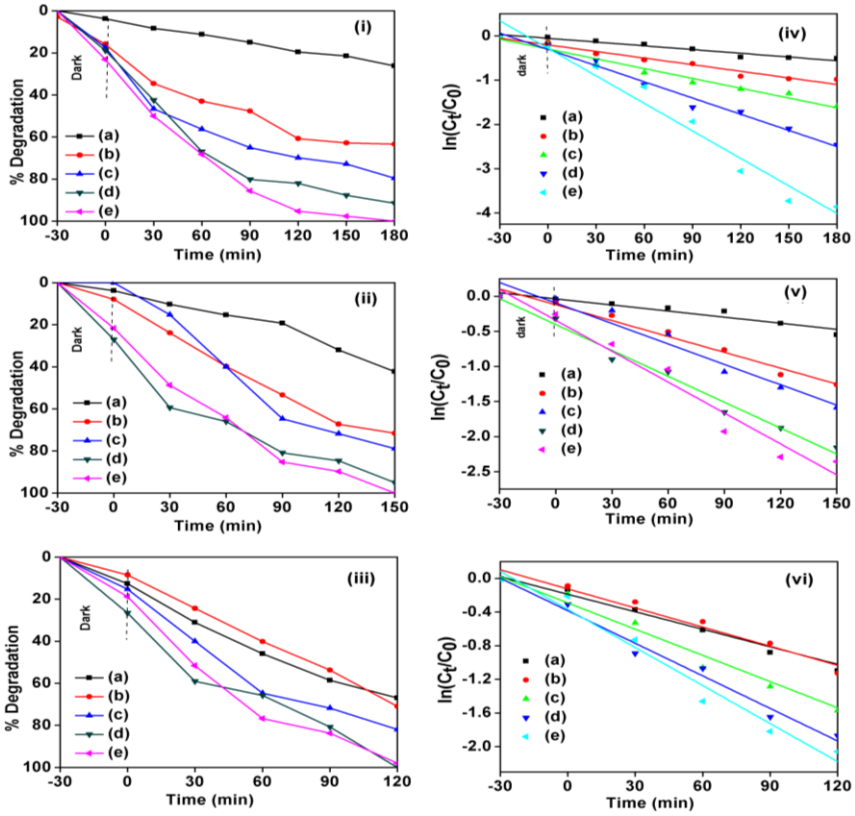

Fig. 7. The graph of time Vs % conversion of (i) RR (ii) MB (iii) 3CP and kinetic plots of time Vs % $\ln(C_t/C_0)$ of the (iv) RR (v) MB (vi) 3CP for the (a) $ZnNb_0$ (b) $ZnNb_1$ (c) $ZnNb_3$ (d) $ZnNb_5$ and (e) $ZnNb_7$.

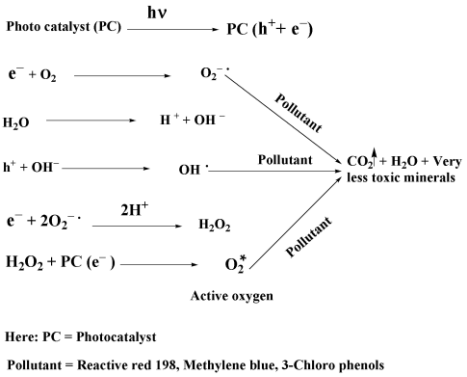

Fig. 8. The proposed radical-ions mechanism for RR, MB and 3CP degradation.

This acidity enhances the formation of active radical limits during the the $^{\bullet}OH$ radicals increases the catalytic activity. The generated peroxy radicals react with oxides of Nb leading to the formation of nascent oxygen [**44].** This happens, when the reduction of Nb(V) to lower oxidation states. This results the highly active oxygen for the degradation of RR, MB and 3CP. Under visible light the conduction band of ZnNb composites create charge vacancy h^+ in the valence molecules. These radicals interact with niobium metal and produce the nascent oxygen, which cause the degradation of dye molecules band during the formation of hydroxy radicals and peroxide **[45]**.

The pentavalent oxidation state of Nb provides multiple electrons to vary the electrical conductivity. The Nb^{+5} induced the formation of oxygen vacancy sites. Hence, the valence difference leads to the degradation of the organic pollutants. The proposed radical-ions mechanism for RR, MB and 3CP degradation is given in **Fig. 7**. The degradation of the enlisted organics to carbon dioxide, water, other very less toxic minerals such as ammonia, nitrates and sulphates **[46-49].**

The catalytic studies of recycled and reused catalyst

The each recovered catalyst from the reaction was collected by nano-filteration and washed with the water, ethanol mixture and dried at 130 °C for 2 h. The recovered

catalysts were subjected to Raman spectra, powder XRD and DRS/UV-Visible spectra (**Fig. S7-S9).** This spectral analysis confirms the stability of the photocatalyst. Thus recovered catalysts spectral data provided in the supporting information. The overall percentage of the degradation was studied in the three cycles and given in the **Fig. S10.** It reveals the degradation and efficiency of the reused catalysts comparatively same as fresh catalyst.

Conclusion

The composites $ZnNb_0$, $ZnNb_1$, $ZnNb_3$, $ZnNb_5$ and $ZnNb_7$ were synthesized in simple insitu chemical method. This formation of the composites was confirmed by FTIR and Raman spectra. The crystallite size and the encapsulation of niobium oxide in zinc oxide frame work were confirmed by XRD, SEM/EDAX and effective doping of niobium oxide and unaffected morphology of zinc oxide nanorods. Thermal stability of composites were analysed by TGA/DTG method. BET/N_2 isotherms of composites reveal the higher surface area with slight variation in its average pore diameter. The particle size also increased slightly with decrease in surface area. The synthesized composite material was used as photo catalyst in the degradation of reactive red, methylene blue and chlorophenol under visible light irradiation. The ZnNb composite shows the percentage of degradation was higher and the kinetic parameters obey *pseudo*-first order oxidation reaction. The recycled and purified composites catalytic activity was compared with the fresh catalyst. This study may leads to improve the research scope in development of photocatalyst for visible light driven reactions. The refractory metal doped ZnO has good visible light absorption these composites could be applicable as photocatalyst in visible light.

Acknowledgements

The authors are thankful to G. Bhaskar Raju, Chief Scientist, CSIR-NML Madras Complex, Chennai, India, for their support during experimental work. The authors are grateful to Dr. T. Sasipraba, Dean, Sathyabama University for her constant support.

Appendix A. Supplementary data

The Particles size graphs, DRS UV-visible, TGA/DTG patterns, FESEM-EDAX Pattern, the recovered catalysts XRD, DRS Raman overall percentage of conversion were given in the supplementary data.

Reference

1. Lang, X.; Chen, X.; Zhao, J. *Chem. Soc. Rev*. **2014**, *43*, 473. **DOI:** 10.1039/C3CS60188A
2. Gompel, D.; Tahir, M.N.; Panthofer, M.; Mugnaioli, E.; Brandscheid, R.; Kolb, U.;Tremel, W. *J. Mater. Chem. A*: **2014**, *2*, 8033. **DOI:** 10.1039/C4TA00183D
3. Li, Y.; Gou, H.; Wang, J.C. *Int. J. Hydrogen Energy* **2014**, *39*, 13481 **DOI:** 10.1016/j.ijhydene.2014.03.023
4. Reddy, G.R.; Chennakesavulu, K. *J. Mole. Struct*. **2014**, *1075*, 406. **DOI:** 10.1016/j.molstruc.2014.06.090
5. Bafrooei, H.B.; Nassaj, E.T.; Ebadzadeh. T.; Hu, C.F. *J. Mater. Sci: Mater. Electron*. **2014**, *25*, 1620. **DOI:** 10.1007/s10854-014-1774-9
6. Muthirulan, P.; Devi, C.K.N.; Sundaram M.M. *Adv. Mat. Lett*. **2014**, *5*, 163. **DOI:** 10.5185/amlett.2013.7507
7. Srivastava, R.; and Yadav, B.C. *Adv. Mat. Lett*. **2012,** *3*, 197. **DOI:** 10.5185/amlett.2012.4330
8. Aegerter, M.A. *Sol. Energy Mater. Sol. Cells*. **2001**, *68*, 401. **DOI:** 10.1016/S0927-0248(00)00372-X
9. Priyanka.; Srivastava, V.C. *Ind. Eng. Chem. Res.* **2013,** *52*, 17790. **DOI:** 10.1021/ie401973r
10. Kuriakose. S.; Satpati B; S. Mohapatra, *Adv. Mat. Lett*. **2015**, *6(3)*, 217. **DOI:** 10.5185/amlett.2015.5693
11. Parlett, C.M.A.; Wilson, K.; Lee, A.F. *Chem. Soc. Rev.* **2013**, *42*, 3876. **DOI:** 10.1039/C2CS35378D
12. Mardani H.R.; Forouzani M; Ziari M.; Biparva P. *Spectrochim. Acta, Part A*, **2015,** *141*, 27. **DOI:**10.1016/j.saa.2015.01.034
13. Esmaeili A,; Kalantari M; *Desalination Water Treat.*, **2015**, *Article in press.* **DOI:** 10.1080/19443994.2015.1010237
14. Zhou, W.; Liu, Y.; Guo, J.; Wu, P. *J. Alloys Compd.*, **2015,** *621*, 423. **DOI:** 10.1016/j.jallcom.2014.10.022
15. Ramachandran D; . Raj N. N, Brijitta. J; Jayanthi V, . Rabel A. M, *ICANMEET Proc.* Chennai, **2013**, 566. **DOI:** 10.1109/ICANMEET.2013.6609366.
16. Deman, H.; Yongmin, Li.; Wenping, J. *Adv. Mat. Lett.* **2010,** *1*, 188. **DOI:** 10.5185/amlett.2010.7137
17. Chennakesavulu.K.; Raju.G.B; Prabhakar. S. *J. Phy.Org.Chem*. **2010**, *23*, 723. **DOI:** 10.1002/poc.1641
18. Nowak, I.; Ziolek, M.; *Chem. Rev.* **1999**, *99*, 3603. **DOI:** 10.1021/cr9800208
19. Lihitkar, P. B.; Violet, S.; Shirolkar, M.; Singh, J.; Srivastava, N.; Naik, R. H.; Kulkarn, K. *Mater. Chem. Phys.* **2012**, *133*, 850. **DOI:** 10.1016/j.matchemphys.2012.01.106
20. Tielens, F. *J Mol Struct Theochem*. **2009,** *903*, 23. **DOI:** 10.1016/j.theochem.2008.09.045
21. Xu, L.; Wang, Y.; Yang, X.; Yu, X.; Guo, Y.; Clark, J. H. *Green. Chem.* **2008,** *10*, 746. **DOI:** 10.1039/B803220C
22. Wojtaszek. A.; Ziolek. M.; Tielens. F. *J. Phys. Chem. C.* **2012,** *116*, 2462. **DOI:** 10.1021/jp208638k
23. Prakash. A.M.; Kevan. L. *J. Am. Chem. Soc.* **1998,** *120*, 13148. **DOI:** 10.1021/ja982262v
24. Lv. A.Y.; Yu. L.; Huang. H.; Feng; Y.; Chen, D.; Xie, X. *Nanotechnology* **2012,** *23*, 065402. **DOI:** 10.1088/0957-4484/23/6/065402
25. Xiao, S.; Liu, L.; Lian, J.; *J. Mater. Sci. Mater. Electron.* **2014,** *25*, 5518. **DOI:** 10.1007/s10854-014-2338-8
26. Tanmay K. G; Prasanta D. *Adv. Mat. Lett.* **2013**, *4*, 121. **DOI:** 10.5185/amlett.2012.7382
27. Chennakesavulu K.; Reddy. M.M.; Reddy. G.R.: Rabel A.M, Brijitta J; Vinita V; Sasipraba T; Sreeramulu J. *J. Mole. Struct*. **2015,** *1091*, 49. **DOI:** 10.1016/j.molstruc.2015.02.052
28. Bacsa, R.R.; Ghys. J.D.; Verelst, M.; Falqui, A.; Machado, B.; Bacsa, W. S.; Chen, P.; Zakeeruddin, S.M.; Graetzel, M.; Serp, P. *Adv Funct Mater* **2009**, *19*, 875. **DOI:** 10.1002/adfm.200801049
29. Lee, C. W.; Park, H. K.; Park. S.; Han, H.S. Seo, S.W. Song, H.J. Shin S. Kim, D.W. Hong, K.S. *J Mater Chem A.* **2015**, *3*, 825. **DOI:** 10.1039/C4TA05885B
30. Xue, X.; Ruan, W.; Yang, L.; Ji. W.; Xie,; Y.; Chen, L.; Song, W.; Zhaoa, B; Lombardi, J. R. *J. Raman Spectrosc* **2012**, *43*, 61. **DOI:** 10.1002/jrs.2988
31. Li, L.; Deng, J.; Yu, R.; Chen, J.; Wanga. Z.; Xing, X. *J. Mater. Chem: A.* **2013**, *1*, 11894. **DOI:** 10.1039/C3TA12599H
32. Kansal, S.K.; Lamba, R.; Mehta, S.K.; Umar. A.; *Mater. Lett*. **2013**, *106*, 385. **DOI:** 10.1016/j.matlet.2013.05.074
33. Mondal, C.; Pal, J.; Ganguly, M.; Sinha, A. K.; Jana, J.; Pal. T. *New J. Chem.* **2014**, *38*, 2999. **DOI:** 10.1039/c4nj00227j
34. Wu, J.; Wang, J.; Li. H.; Du. Y.; Jia, X.; Liu, B. *Cryst.Eng.Comm.* **2014**, *16***,** 9675. **DOI:** 10.1039/C4CE01213E
35. Ahmad, M.; Ahmed. E; Hong. Z. L.; Ahmed. W.; Elhissi. A.; Khalid. N. R. *Ultrason. Sonochem*. **2014**, *21*,761. **DOI:** 10.1016/j.ultsonch.2013.08.014

36. Tian. J.; Zhang, Q.; Zhang, L.; Gao. Shen. L.; Zhang. S.; Qua, X.; Cao, G. *Nanoscale* **2013**, *5*, 936. **DOI:** 10.1039/C2NR32663A
37. Fakhri, H.; Mahjoub. A. R.; Cheshme, A.H.K. *Appl. Surf. Sci*. **2014**, *318*, 65. **DOI:**10.1016/j.apsusc.2014.01.024
38. Polsongkram, D.; Chamninok, P.; Pukird, S.; Chow, L.; Lupan, O.; Chai, G.; Khallaf, H.; Park, S.; Schulte, A. *Physica B.* **2008**, *403*, 3713. **DOI:** 10.1016/j.physb.2008.06.020
39. Kuriakose, S.; Satpatib, B.; Mohapatra. S.; *Phys. Chem. Chem. Phys*. **2014**, *16*, 12741. **DOI:** 10.1039/c4cp01315h.
40. Uchida, M.; Okuwaki, A. *J. Solution Chem*. **2003**, *32*, 19. **DOI:** 10.1023/A:1022980614320
41. Li, R.; Ren, X.; Wei, H. M.; Feng, X.; Lin, Z.; Li, X.; Hu, C.;Wang. B. J. *Mater. Chem: A*. **2014**, *2*, 5724. **DOI:** 10.1039/C3TA15058E
42. Li, W.; Li, D.; Wang, J.; Shao, Y.; You, J.; Teng, F. *J. Mol. Catal:A. Chem*. **2013**, *380*, 10. **DOI:** 10.1016/j.molcata.2013.09.001
43. Zhang, Y., Zhou. L.; Tan, C. *J. Photochem. Photobiol:B*. **2014**, *134*, 9. **DOI:** 10.1016/j.jphotobiol.2014.03.022
44. Guo, M.Y.; Ng, A. M. C.; Liu, F.; Djurisi, A. B.; Chan W. K. *Appl. Catal: B Environ*. **2011**, *107*, 150. **DOI:** 10.1016/j.apcatb.2011.07.008
45. Ziolek, M.; Sobczak. I.; Decyk. P; Wolski, I. Catal. Commun. **2013**, *37*, 85. **DOI:** 10.1016/j.catcom.2013.03.032
46. Her, N.; Park, J. S.; Yoon, J.; Sohn, J.; Lee, S.; Yoon, Y.; *Ind. Eng. Chem. Res*. **2011**, *50*, 6638. **DOI:** 10.1021/ie102419v
47. Czaplicka, M. *J. Hazard. Mater*. **2006**, *134*, 49. **DOI:** 10.1016/j.jhazmat.2005.10.039
48. Breault, T.M.; Bartlett, B. M. *J. Phys. Chem. C*. **2013**, *117*, 8611. **DOI:** 10.1021/jp312199t
49. Reddy, G.R.; Balasubramanian, S.; Chennakesavulu. K. *J. Mater. Chem*. A. **2014**, *2*, 15598. **DOI:** 10.1039/C4TA01869A

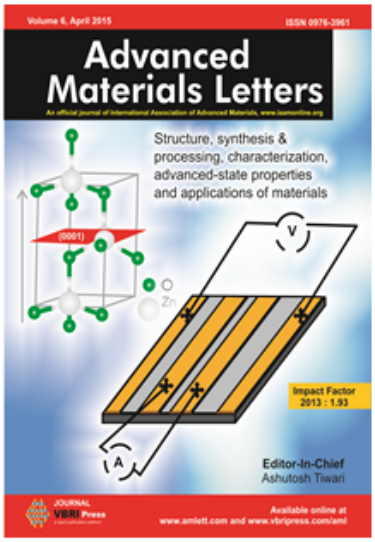

Supporting data

Visible light driven photocatalytic degradation of the reactive red-198, methylene blue and 3-chloro phenol by Nb_2O_5@ZnO composites: Synthesis and characterization

K. Chennakesavulu[1*], G. Ramanjaneya Reddy[2], S. Sanjeevi Prasath[3], S. Supriya[1], S. Sivanesan[3]

[1]*Department of Chemistry & Centre of Excellence in Energy Research, International Research Centre, Sathyabama University, Jeppiaar Nagar, Chennai 600 119, India*
[2]*Department of Inorganic Chemistry, School of Chemical Sciences, University of Madras, Guindy Campus, Chennai 600 025, India*
[3]*Centre for Nanoscience and Nanotechnology, International Research Centre, Sathyabama University, Chennai 600 119, India*

[*]Corresponding author. Tel: (+91) 4424503814; E-mail: chennanml@yahoo.com

Table of contents:

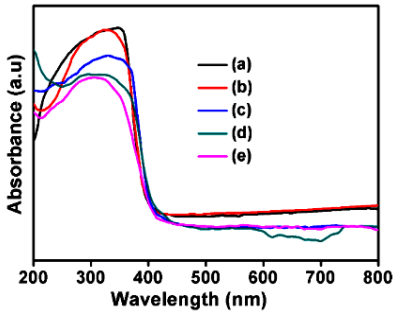

Fig. S1. DRS/UV-Visible spectra of the (a) $ZnNb_0$ (b) $ZnNb_1$ (c) $ZnNb_3$ (d) $ZnNb_5$ and (e) $ZnNb_7$.

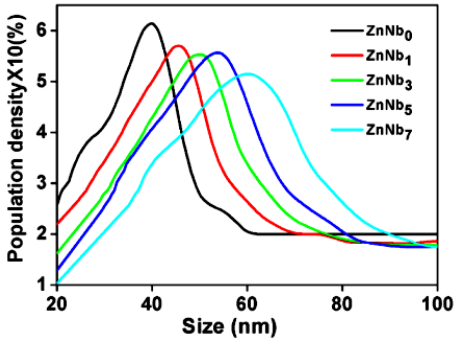

Fig. S2. Particle size distribution curves of composites, which were obtained by zeta acoustic sizer (Acoustic method, 2 wt% to 5 wt % of samples was dispersed in water during the measurement).

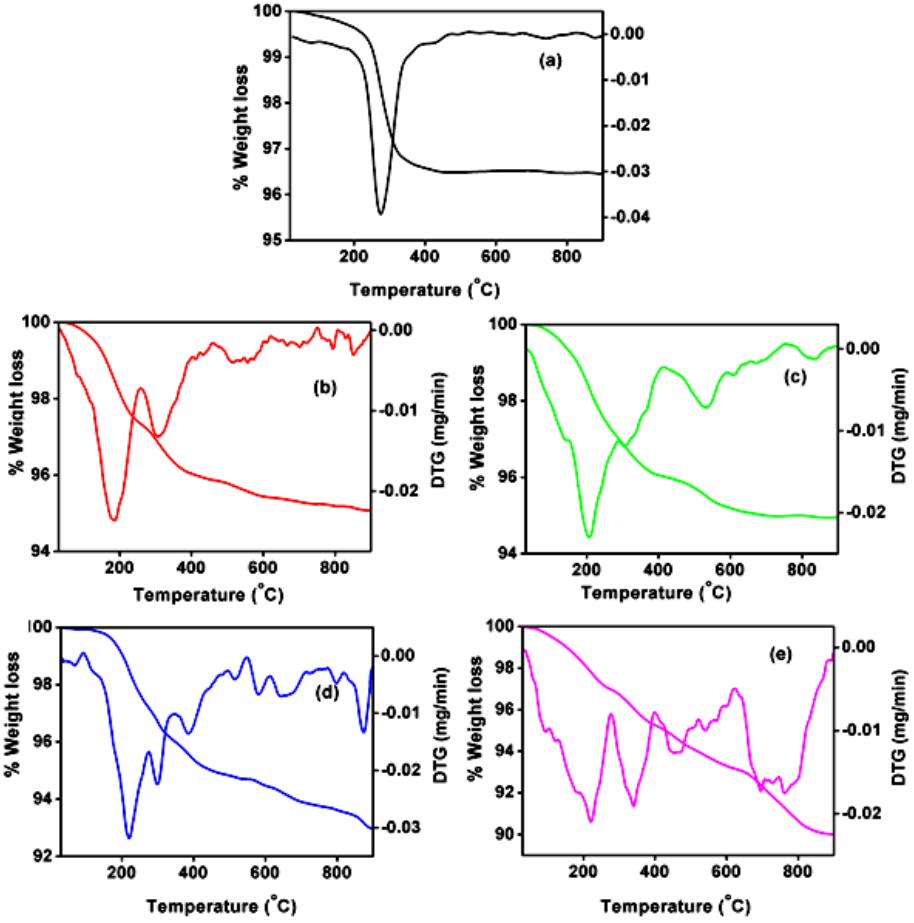

Fig. S3. TG/DTG patterns of the (a) $ZnNb_0$ (b) $ZnNb_1$ (c) $ZnNb_3$ (d) $ZnNb_5$ and (e) $ZnNb_7$.

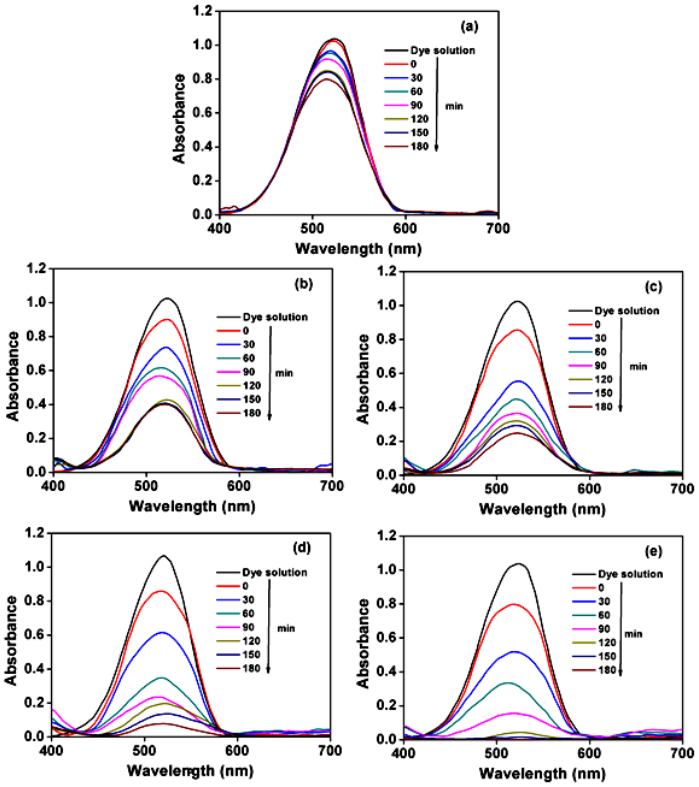

Fig. S4. The absorption plots for the photo degradation of RR in the presence of (a) $ZnNb_0$ (b) $ZnNb_1$ (c) $ZnNb_3$ (d) $ZnNb_5$ and (e) $ZnNb_7$ under visible light irradiation.

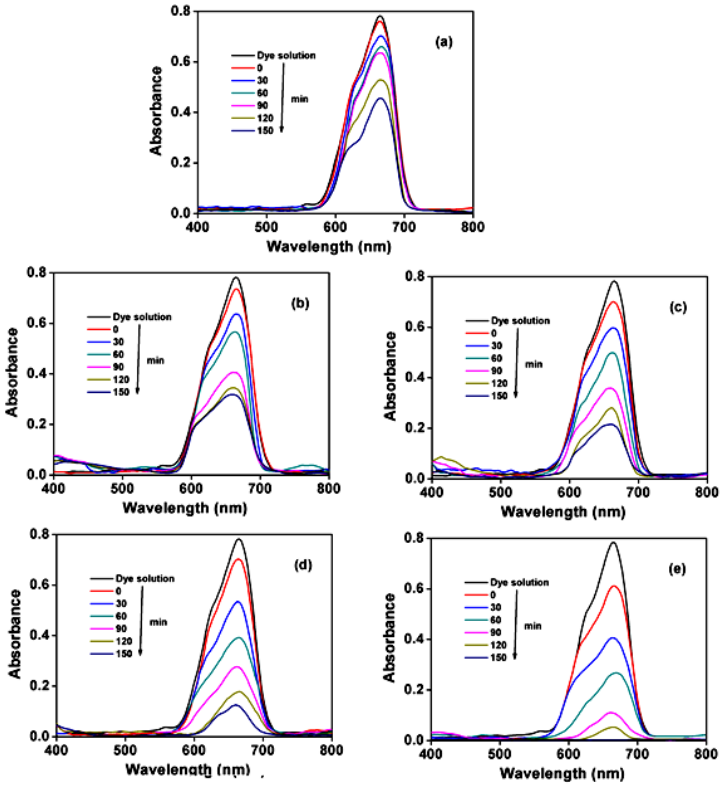

Fig. S5. The absorption plots for the photo degradation of MB in the presence of (a) $ZnNb_0$ (b) $ZnNb_1$ (c) $ZnNb_3$ (d) $ZnNb_5$ and (e) $ZnNb_7$ under visible light irradiation.

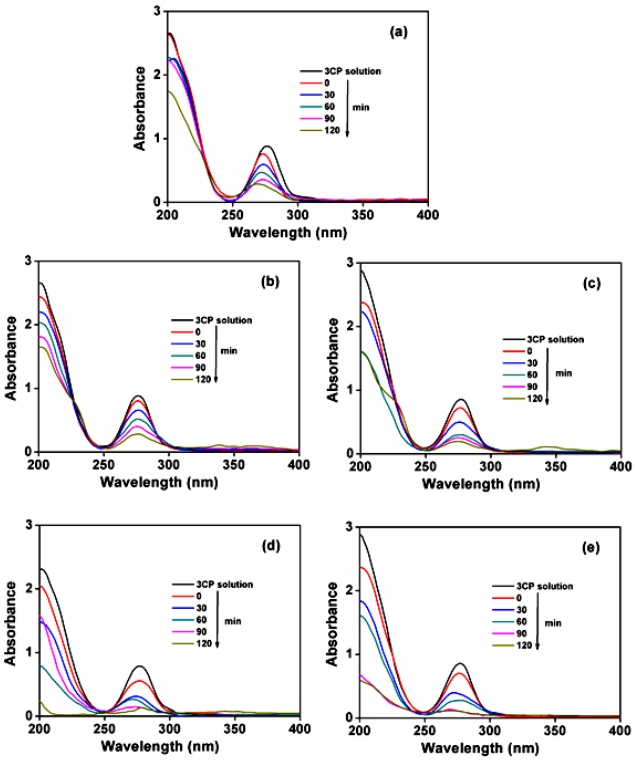

Fig. S6. The absorption plots for the photo degradation of 3CP in the presence of (a) $ZnNb_0$ (b) $ZnNb_1$ (c) $ZnNb_3$ (d) $ZnNb_5$ and (e) $ZnNb_7$ under visible light irradiation.

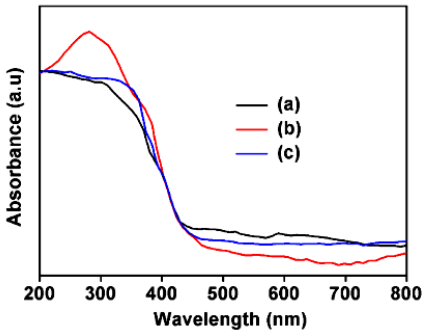

Fig. S7. The DRS spectra of recovered (a) $ZnNb_0$ (b) $ZnNb_3$ and (c) $ZnNb_7$

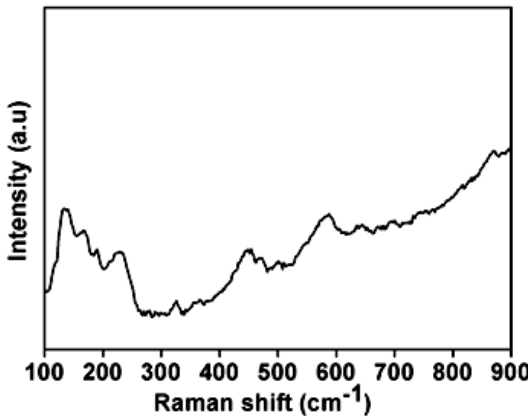

Fig. S8. Raman spectrum of the composite $ZnNb_5$.

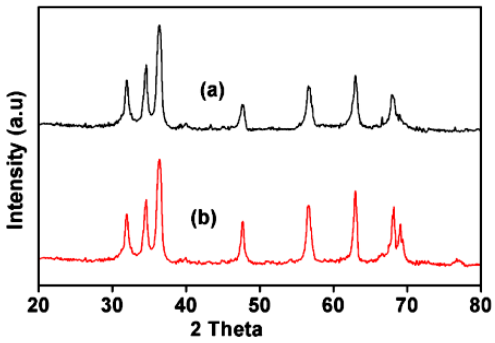

Fig. S9. The powder XRD patterns of recovered (a) $ZnNb_1$ and (b) $ZnNb_3$.

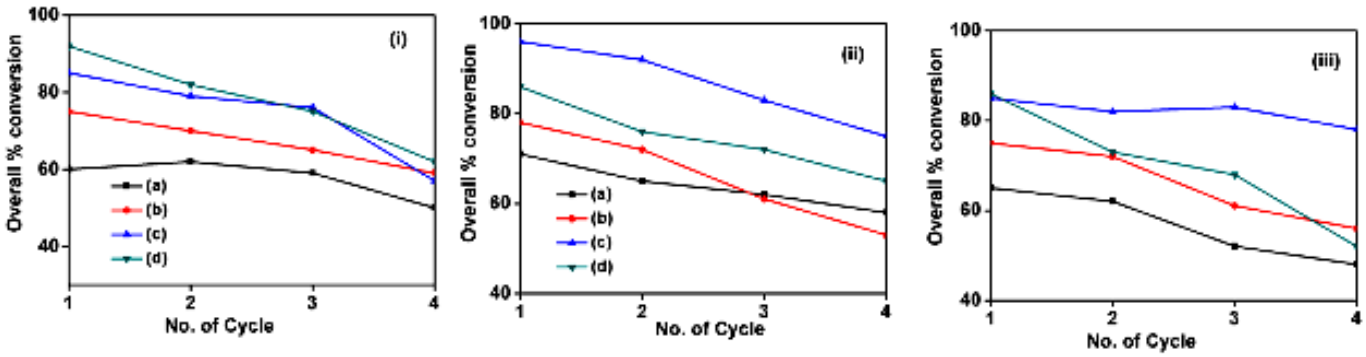

Fig. S10. The plots of No. of Cycle Vs overall percentage of conversion for the (i) RR (ii) MB, (iii) 3CP.

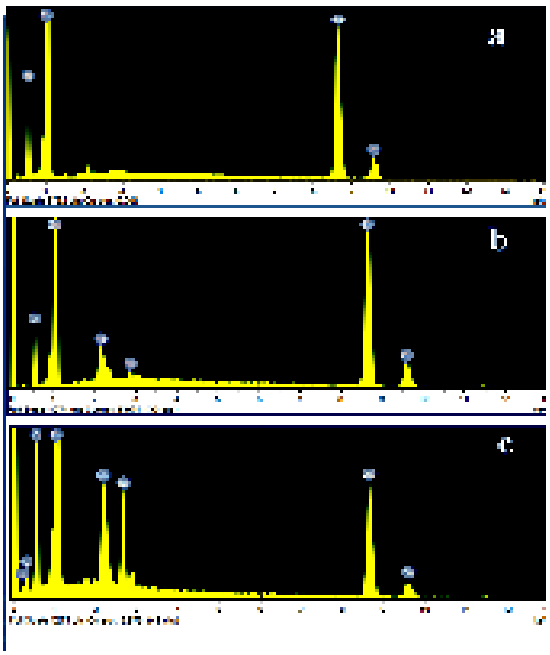

Fig. S11. FESEM/EDAX patterns of given compounds.

